B. Shome[1]
Research Associate.

L.-P. Wang[2]
Assistant Professor.
LWANG@ME.UDEL.EDU

M. H. Santare
Associate Professor.

A. K. Prasad
Associate Professor

A. Z. Szeri
Professor.

Department of Mechanical Engineering,
University of Delaware,
Newark, DE 19716-3140

D. Roberts
President,
Anatek, Inc.,
Kennett Square, PA 19348

Modeling of Airflow in the Pharynx With Application to Sleep Apnea

A three-dimensional numerical modeling of airflow in the human pharynx using an anatomically accurate model was conducted. The pharynx walls were assumed to be passive and rigid. The results showed that the pressure drop in the pharynx lies in the range 200–500 Pa. The onset of turbulence was found to increase the pressure drop by 40 percent. A wide range of pharynx geometries covering three sleep apnea treatment therapies (CPAP, mandibular repositioning devices, and surgery) were modeled and the resulting flow characteristics were investigated and compared. The results confirmed that the airflow in the pharynx lies in the laminar-to-turbulence transitional flow regime and thus, a subtle change in the morphology caused by these treatment therapies can significantly affect the airflow characteristics.

Introduction

It has been estimated that 40 million Americans suffer from various forms of sleep disorders, which can have a significant impact on health, quality of life, and productivity. These disorders can lead to debilitating cardiovascular diseases, lowered productivity in the work place, and increased risks of fatigue-related accidents (Leger, 1994). The National Commission on Sleep Disorders Research (1993) estimated the indirect costs of sleep disorders to the general population to be as high as $15 billion per year. It has been estimated (Pack, 1993) that around 4 percent of the middle-aged population in the U.S. meet the minimum clinical definition of Obstructive Sleep Apnea (OSA), which is the most serious form of sleep disorder in terms of mortality and morbidity.

With few exceptions, OSA is associated with snoring, the mechanics of which appear to involve vibration of the free margin of the soft palate and/or walls of the pharynx, and are linked to flaccidity of the palatal muscles during sleep. A supine posture, which allows both the soft palate and tongue to fall into the airstream, exacerbates this condition, as does obesity and/or hyperdevelopment of these soft-tissue structures relative to the dimensions of the pharynx and oral cavity. However, even heavy snoring is not necessarily indicative of the existence of OSA, which probably has a multifactorial etiology, including central nervous system dysfunctions. The peripheral mechanics leading to narrowing of the phayrngeal space, and its eventual collapse and obstruction, has been studied empirically by Isono and Remmers (1993), who interpreted their findings in terms of the physics governing collapsible tubes. They showed that the caliber (cross-sectional area) of the pharynx is a function of its wall structures (compliance) and intraluminal air pressures. For intermediate ranges of *transmural* pressure (luminal or internal pressure minus external pressure exerted by the wall) the caliber varies. Where the walls are very compliant, even a small intraluminal pressure drop may cause a large change in cross-sectional area. At large positive values of transmural pressure the pharynx is distended and stiff and at large negative values, the cross-sectional area is greatly reduced and may become zero (collapse).

There are, therefore, a number of parameters that must be taken into account when attempting to characterize or predict OSA. These include morphology (in its general sense, which includes both topology and histological structure of the walls) and knowledge of the local airflow and pressure distribution within the pharynx. In general, the airflow characteristics depend on the velocity and acceleration of the air, the geometry of the pharynx, the nature (laminar, transitional, or turbulent) of the flow, and on the volumetric flow rate. In addition, three-dimensional flow features such as separation and transition from laminar to turbulent flow could affect the flow pressure significantly.

The majority of the previous work on collapsible tubes (Kamm and Pedley, 1989) and nasal cavities (Keyhani et al., 1993) has dealt with laminar flows, while the airflow in bronchial airways has been assumed fully developed turbulent flow (Elad et al., 1987). Recently, Hahn (1992), based on experimental measurements, has demonstrated that the air flow inside the nasal cavity is laminar for low flow rates and turbulent for medium or high flow rates. Thus, transition from laminar to turbulent flow in the airway could occur during heavy breathing or due to partial obstructions in the pharynx. The transition process could significantly increase the pressure drop, thereby increasing the likelihood of airway collapse. Moreover, since the flow Reynolds number could span the critical range, a slight

[1] Current address: PPG Industries, Inc., FGRC/RID, P.O. Box 2844, Pittsburgh, PA 15230-2844.

[2] Corresponding author.

Contributed by the Bioengineering Division for publication in the JOURNAL OF BIOMECHANICAL ENGINEERING. Manuscript received by the Bioengineering Division November 25, 1996; revised version received December 16, 1997. Associate Technical Editor: J. B. Grotberg.

change in the pharynx geometry may lead to significant changes in the airflow characteristics, possibly causing OSA.

Detailed information about the airflow characteristics in the pharynx is lacking. The majority of the previous work on modeling of airflow in the upper airway has been mostly limited to the nasal cavity (Elad et al., 1991; Keyhani et al., 1993, among others). Thus, little is known about the relationship between the airflow pressure distribution, volumetric flow rate, and the pharynx geometry.

There exist various therapies (both reversible and irreversible) for treating OSA. Continuous positive air pressure (CPAP), dental repositioning devices, and pharyngeal surgery are the most widely used treatment therapies. However, little is known about the effect of these therapies on the airflow characteristics and whether their use leads to favorable airflow characteristics conducive to the prevention of OSA. Thus, the information on how these treatment therapies affect the airflow characteristics could broaden the range and type of diagnostic information. Such diagnostic information could lead to better treatment therapy planning, as well as improving the cost-effectiveness of diagnosis and treatment of OSA. In addition, in the case of irreversible therapies (such as pharyngeal surgery), the availability of pre-operative diagnostic information would help in presurgical planning and analysis. The availability of such presurgical diagnostic information has the potential for lowering the failure rate (as high as 50 percent) associated with pharyngeal surgery-based treatment therapy.

Thus, the main objectives of this study were to: (*i*) conduct three-dimensional modeling of airflow in pharynx using anatomically accurate geometry, (*ii*) investigate the effect of turbulence and airflow rate on the airflow characteristics, and (*iii*) investigate the effect of various treatment therapies on the local airflow characteristics.

Numerical Modeling

Model Description. A three-dimensional numerical model of airflow in the pharynx was constructed using an anatomically accurate geometry. As a first step toward a better understanding of the airflow in the complex geometry, the pharynx walls were assumed to be passive and rigid and the flow was assumed to be incompressible and steady. The results presented here will serve as a basis to compare with the more realistic study of dynamically coupled, soft-tissue airflow interactions, which is to be carried out in the near future. It should be noted that both the unsteadiness and flexible boundary may play important roles in airway collapse (Tutty and Pedley, 1994; Luo and Pedley 1996, Lynch and Pedley 1996, Carew and Pedley, 1997) and thus the occurance of apnea. The governing equations for the conservation of mass (continuity) and momentum (Navier–Stokes) with the assumptions given above are:

$$\frac{\partial \bar{u}_i}{\partial x_i} = 0 \tag{1}$$

$$\bar{u}_j \frac{\partial \bar{u}_i}{\partial x_j} = -\frac{1}{\rho}\frac{\partial p^*}{\partial x_i} + \frac{\partial}{\partial x_j}\left[(\nu + \nu_t)\left(\frac{\partial \bar{u}_i}{\partial x_j} + \frac{\partial \bar{u}_j}{\partial x_i}\right)\right] \tag{2}$$

where $\bar{u}_i$ is the Reynolds-averaged velocity field, p^* is the modified pressure $p^* \equiv p + \rho\overline{u_i' u_i'}/3$, and u_i' is the turbulent velocity fluctuations. The eddy viscosity ν_t is given as

$$\nu_t = C_\mu \frac{k^2}{\epsilon} \tag{3}$$

and the turbulent kinetic energy, k, and the turbulent dissipation, ϵ, are modeled by the two-equation $k-\epsilon$ model (Launder and Spalding, 1974) as:

$$\bar{u}_j \frac{\partial k}{\partial x_j} = \frac{\partial}{\partial x_j}\left(\frac{\nu_t}{\sigma_k}\frac{\partial k}{\partial x_j}\right) + \nu_t\left(\frac{\partial \bar{u}_i}{\partial x_j} + \frac{\partial \bar{u}_j}{\partial x_i}\right)\frac{\partial \bar{u}_i}{\partial x_j} - \epsilon \tag{4}$$

$$\bar{u}_j \frac{\partial \epsilon}{\partial x_j} = \frac{\partial}{\partial x_j}\left(\frac{\nu_t}{\sigma_\epsilon}\frac{\partial k}{\partial x_j}\right) + C_1 \nu_t \frac{\epsilon}{k}\left(\frac{\partial \bar{u}_i}{\partial x_j} + \frac{\partial \bar{u}_j}{\partial x_i}\right)\frac{\partial \bar{u}_i}{\partial x_j} - C_2\frac{\epsilon^2}{k} \tag{5}$$

where $C_\mu = 0.09$, $C_1 = 1.44$, $C_2 = 1.92$, $\sigma_k = 1.0$, and $\sigma_\epsilon = 1.3$. The air density ρ was set to 1.2 kg/m^3 and the dynamic viscosity used was 1.8×10^{-5} N·s/m^2.

At the pharynx walls, the no-slip boundary condition (i.e., $\bar{u}_i = 0$) was applied. It is well known that the $k-\epsilon$ model leads to significant errors in the near-wall region due to strong viscous effects and departures from local isotropy (Hanjalic, 1994). Therefore, the k and ϵ equations are not solved in the near-wall region. Instead, the variation of turbulent diffusivity is modeled using van Driest's mixing length approach (FIDAP, 1993). The inlet was assumed to have a uniform plug flow velocity profile corresponding to an average inspiratory flow rate of 4×10^{-4} m^3/s. We also assumed a uniform profile for both the turbulent kinetic energy k and the dissipation rate ϵ at the inlet. The value of k at the inlet was set to 5 percent of the inlet flow speed, a value in accordance with recent observation in the nasal cavity by Hahn (1992). The value of ϵ was calculated from k and a length scale defined as the hydraulic diameter at the inlet. At the outlet, a stress-free boundary condition, which arises naturally from the application of finite element method, was used. These governing equations, along with the boundary conditions, were solved using the commercial finite element software FIDAP (Fluid Dynamics International) to obtain the velocity and pressure fields.

Mesh Generation. The finite element mesh, consisting of eight-noded brick elements, was constructed from Magnetic Resonance Imaging (MRI) scans by digitizing scanned images of the pharynx using the APIS software developed by Anatek, Inc. The relative orientation of the pharyngeal cross sections and geometric coordinates of points that define the bounding curve of each cross section were first determined. This information was then input into the mesh-generation module of FIDAP. We divided the boundary of each section into four parts, which defined the four dividing points. Straight lines were then used to link the dividing points between two consecutive sections. Two to three nodal points were added to each of the straight

Nomenclature

A_{cs} = cross-sectional area of pharynx
C_1, C_2, C_μ = constants in turbulence model
d = effective pharynx diameter
k = turbulence kinetic energy
p = pressure
p^* = effective pressure = $p + \rho\overline{u_i' u_i'}/3$
$\bar{p}$ = volume-averaged pressure
Q = inspiratory flow rate
Re = Reynolds number = $\bar{u}_{in} d/\nu$
s = distance along pharynx axis measured from soft palate
$\bar{u}_i$ = Reynolds-averaged velocity
$\bar{u}_{in}$ = average inlet velocity
u_i' = velocity fluctuation
x_i = coordinate
Δp = pressure drop
ϵ = turbulence viscous dissipation rate
ν = kinematic viscosity
ν_t = turbulent eddy viscosity
ρ = density
σ_k, σ_ϵ = constants in turbulence model

Subscripts

i = direction
in = inlet

/ 9711$$ju14 04-13-98 22:42:43 asmel ASME: J Bio Eng

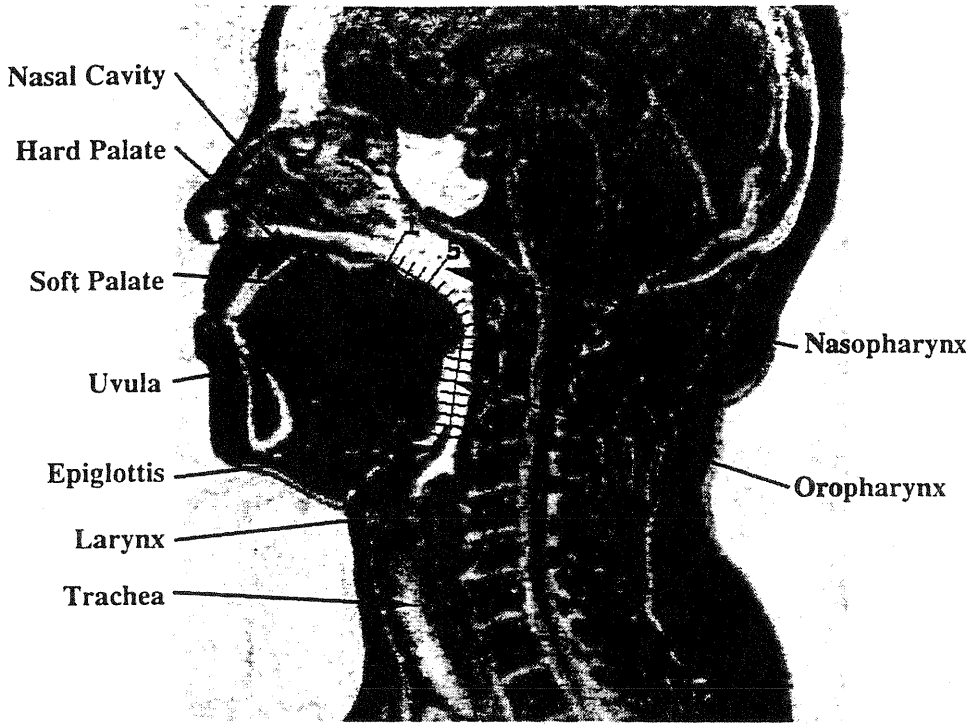

Fig. 1(*a*) A sketch showing the modeled pharynx in relation to the known anatomy of upper airway

line segments. Finally with these nodal points, FIDAP generated the mesh configuration between the sections automatically. Therefore, there is some uncertainty involved in determining the surface geometry between any two consecutive sections. In the current model, 5500 elements were used, since this was found to provide a good trade off between accuracy and computation time. Test simulations showed that the maximum relative error in cross-sectional averaged pressure between 3500 and 5500 elements was typically 5 percent, while increasing the number of elements from 5500 to 7500 changed the solution by less than 2 percent. Therefore, we expect that the numerical error due to mesh resolution at 5500 elements is within 2 to 5 percent.

Figure 1(*a*) shows the particular region of airway that was modeled and its relation with the known anatomy of upper airway. The locations of the 20 individual sections where MRI scans were taken are marked. A typical mesh for a representative pharynx geometry from an OSA patient is shown in Fig. 1(*b*).

Numerical Methods. FIDAP uses the Galerkin form of the method of weighted residuals. In this method, the solution domain (pharynx) is subdivided into a finite number of small domains (elements) and the governing partial differential equations are replaced by discrete, nonlinear algebraic equations within each element. The pressure discretization was based on the penalty function approach, one of the methods used in FIDAP. In this approach the continuity equation, Eq. (1), is replaced by $p^* = -(1/\delta)\partial\bar{u}_i/\partial x_i$. The penalty parameter δ is set to 10^{-6} in our simulations. Provided that δ is small enough, the very slightly compressible system will yield a solution very close to the original incompressible system (for details see the FIDAP 7.0 Theory Manual). These equations were then solved iteratively by a segregated (pressure projection) algorithm until the changes in the velocity and the pressure between successive iterations are less than 0.1 percent. The computations were performed on an IBM RS 6000/990 computer with 512 Mb of CPU memory and the actual computational time varied between 6–8 hours.

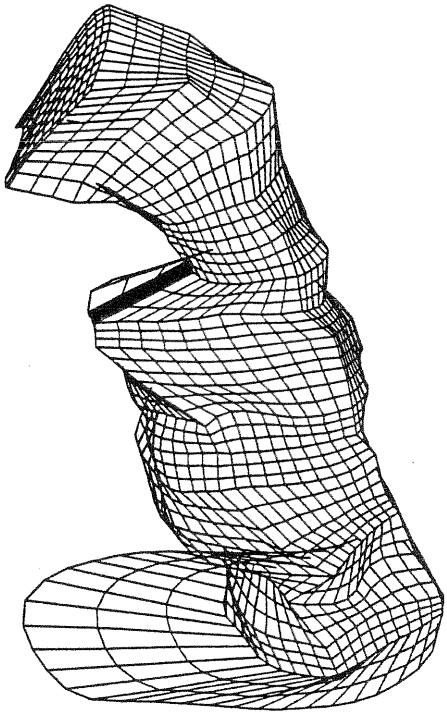

Fig. 1(*b*) Finite element mesh of a representative pharynx from an OSA patient

Assessment of Turbulence Model. The transition from laminar to turbulent flow is characterized by the nondimensional Reynolds number, Re. Usually, transitional flow prevails in the Reynolds number range of $2000 < \mathrm{Re} < 10{,}000$. However, three-dimensional flow features such as flow separation and recirculation might trigger a transition to turbulence at lower Reynolds number. The Reynolds number variation for a typical

/ 9711$$ju14 04-13-98 22:42:43 asmel ASME: J Bio Eng

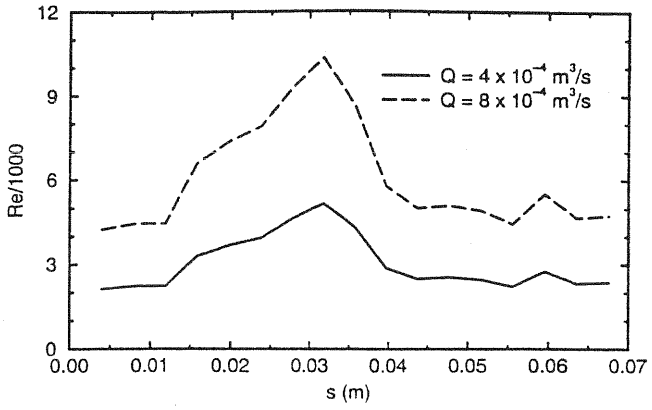

Fig. 2 Variation of Reynolds number in pharynx

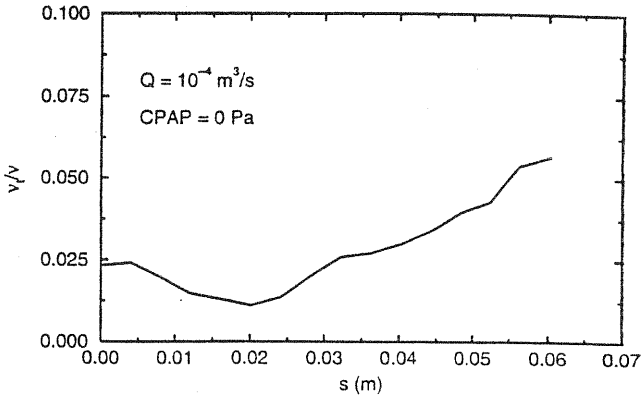

Fig. 4 Variation of the eddy viscosity-to-kinematic viscosity ratio for laminar flow in pharynx

pharynx geometry is shown in Fig. 2 for the average and peak inspiratory flow rate of 4×10^{-4} m^3/s and 8×10^{-4} m^3/s, respectively. The Reynolds number was defined based on the hydraulic diameter, $D = 4A/P$, where A is the cross-sectional area and P is the perimeter. The abscissa, s, is the distance along the pharynx from the soft palate to the epiglottis. Figure 2 shows that for the average flow rate, the flow in the pharynx is in transition from laminar to turbulent flow and could be fully turbulent at peak flow rates where Re could be as high as 10,000. Since the Reynolds number spans the critical range (beyond which the flow becomes turbulent), a slight change in the morphology of the pharynx could considerably affect the airflow characteristics. In fact, this has been observed in this study and will be discussed later.

The flow in the pharynx is mostly in the transitional flow regime; thus, depending on the flow acceleration and deceleration (dictated by the pharynx geometry), it is likely that portions of the flow could be locally laminar and other portions could be locally turbulent. Furthermore, because of the presence of strong flow acceleration, deceleration, and recirculation, transport and history effects are important. In such situations, an accurate and realistic turbulence model would be one that reproduces the limiting laminar and fully turbulent flow behaviors as well as accounting for the transport and history effects. In contrast to zero-equation models (such as the mixing length model), two-equation models (such as $k-\epsilon$, $k-\omega$ model, etc.) take into account the transport and history effects. In addition, two-equation models have been used successfully to predict transitional or low-Reynolds-number turbulent flow (Schmidt and Patankar, 1987; Wilcox, 1994).

In order to assess the ability of two-equation turbulence models to treat transitional flow, two widely used models, namely the $k-\epsilon$ model (Launder and Spalding, 1974) and the $k-\omega$ model (Wilcox, 1994) were considered. As indicated earlier, these models do account for the transport and history effects and have been well tested for modeling of fully developed turbulent flow. Thus, these models were only assessed for their ability to reproduce the limiting laminar flow behavior for sufficiently low Reynolds number situations, where laminar flow prevails. This assessment was conducted for several pharynx geometries with a low inspiratory flow rate of 10^{-4} m^3/s. The maximum Reynolds number for these simulations was around 600 and thus, the flow could be assumed to be laminar. The result for a typical pharynx geometry is shown in Fig. 3 where the turbulence model predictions are compared to that for the laminar flow. The ordinate, Δp, is the pressure drop defined as $\Delta p = \bar{p} - p_{in}$, where $\bar{p}$ is the volume-averaged pressure over the region between two consecutive cross-sectional stations and p_{in} is the inlet pressure at the soft palate. Figure 3 shows that the $k-\epsilon$ model predictions more closely matched the laminar flow results when compared to the $k-\omega$ model. Similar results were observed for other pharynx geometries as well as for several benchmark engineering geometries, such as straight ducts, curved ducts, elbows with various curvatures, etc. On the other hand, the $k-\epsilon$ model has been well tested for fully developed turbulent flow (Launder and Spalding, 1974; Rodi, 1980; Hanjalic, 1994). Therefore, the $k-\epsilon$ model appears to be capable of reproducing the limiting behaviors of both laminar and fully turbulent flow, and is adopted here to simulate the transitional flow in the pharynx. The close agreement between the $k-\epsilon$ model and the laminar predictions also validates the near-wall modeling used in FIDAP. As a further validation, the ratio

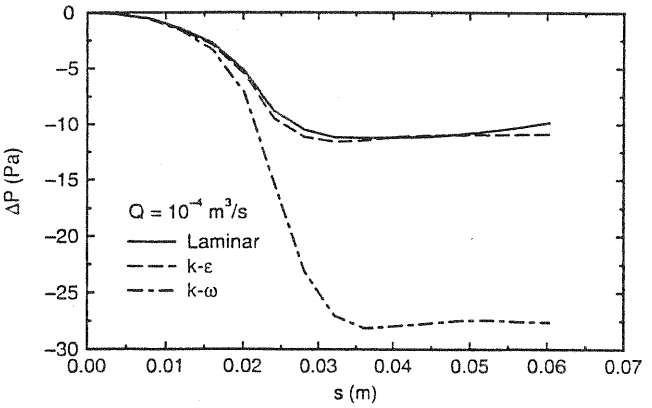

Fig. 3 Comparison of turbulence models for predicting laminar pressure drop in pharynx

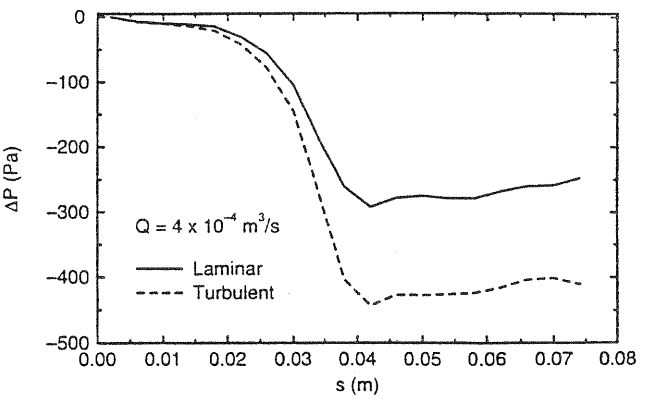

Fig. 5 Effect of turbulence on pressure drop in pharynx

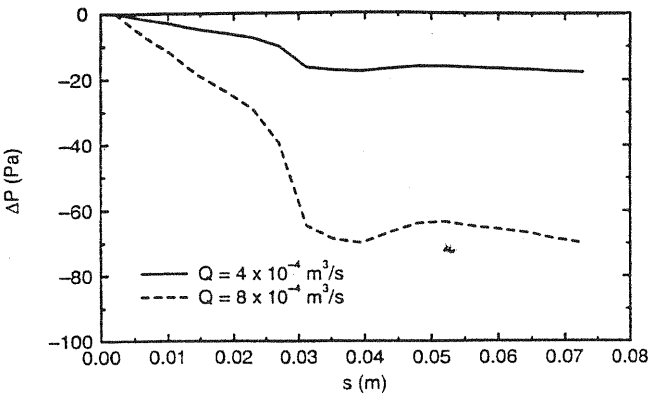

Fig. 6 Effect of inspiratory flow rate on pressure drop in pharynx

of the volume-averaged turbulent viscosity to the kinematic viscosity for the low flow rate case is shown in Fig. 4. As seen in Fig. 4, the magnitude of the viscosity ratio is close to the expected value of zero. One should note, however, that the k–ϵ turbulence model is not accurate for curved flow regions. For predicting the pressure change in this study, it appears to be adequate.

Results and Discussion

In the current study, the airflow in the pharynx was modeled to investigate the effects of turbulence and flow rate on the flow field and pressure drop. In addition, the effects of CPAP, mandibular repositioning devices, and surgical treatment therapies on the airflow characteristics, including the pressure drop, were investigated for an average inspiratory flow rate of 4×10^{-4} m^3/s. The effect of various parameters on the pressure drop profile is important since the pressure drop profile gives the magnitude and location of the minimum intraluminal pressure that exists in the pharynx. This information can be used to help in determining locations where airway collapse is most likely to occur.

Figure 5 shows the effect of turbulence on the pressure drop in a typical pharynx geometry for an apneic patient without any treatment. A laminar flow calculation was also performed as a comparison. The figure shows that the pressure drop could be as high as 500 Pa for an average inspiratory flow rate of 4×10^{-4} m^3/s and as much as 40 percent of this can be accounted for by the onset of turbulence. Turbulence involves vigorous exchange of energy between the high speed core flow and the low speed near-wall flow. This can considerably increase the frictional losses, thereby leading to a large increase in pressure drop.

The effect of inspiratory flow rate on the pressure drop for a typical pharynx geometry of a patient with dental device (8 mm manibular potrusion) is shown in Fig. 6. The two flow rates considered are 4×10^{-4} m^3/s and 8×10^{-4} m^3/s corresponding to the average and peak values. Such an investigation is important since the flow through the airway cycles through a minimum, average, and peak value and it is important to know the sensitivity of the pressure drop to the changes in flow rate. The figure shows that the flow rate has a large effect on the pressure drop. In fact, the pressure drop is observed to vary approximately as the square of the flow rate. It is interesting to note as a comparison, that the pressure drop for a laminar flow in a smooth tube is proportional to the flow rate, Q, while for turbulent flow it is proportional to $Q^{1.75}$ (White, 1986). It is speculated that the complex flow geometry in the pharynx may contribute to the stronger dependence of Δp on Q, observed here. One possible explanation is that the flow here is dominated by inertial effects, whereas in a smooth pipe there is a simple balance between pressure drop and viscous effects.

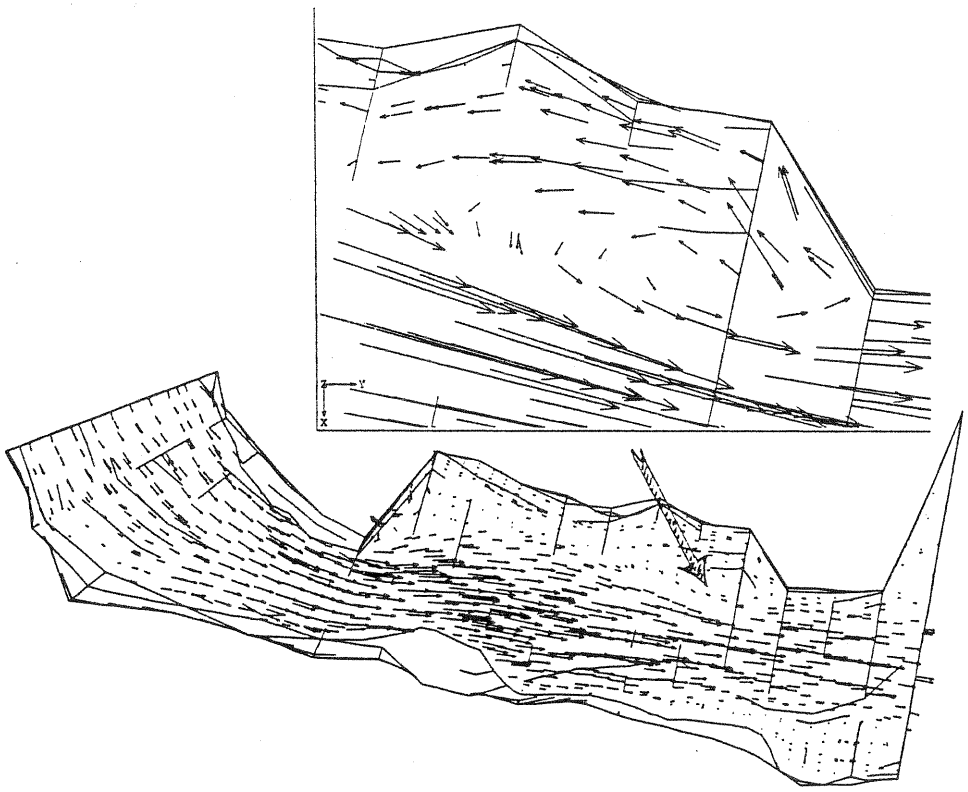

Fig. 7 The full midplane velocity vector plot and an enlarged view of velocity vector field showing recirculation in a surgically altered pharynx

Figure 7 shows an enlarged view of the three-dimensional velocity vector field in a surgically altered pharynx. The figure shown is a typical pharynx geometry after pharyngeal surgery to correct OSA. The figure clearly shows the presence of a flow recirculation zone, which is caused by the abrupt changes in the morphology in the uvula area. Such flow recirculation and separation regions caused by changes in the morphology probably occur also in healthy models and could trigger turbulence and increase the pressure drop.

The effect of CPAP therapy on the airway cross-sectional areas, average velocities, and the corresponding pressure drops for a single patient is shown in Figs. 8(*a*), 8(*b*), and 8(*c*). Like pressure, the average velocity is defined as the local volume-averaged value between two consecutive cross-sectional stations. Analyses were conducted for CPAP levels corresponding to 0, 500, 1000, and 1500 Pa applied to the same patient. The

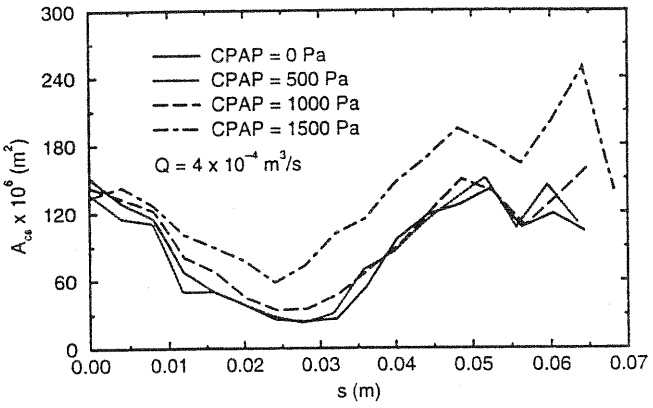

Fig. 8(*a*) Effect of CPAP on the cross-sectional area of pharynx

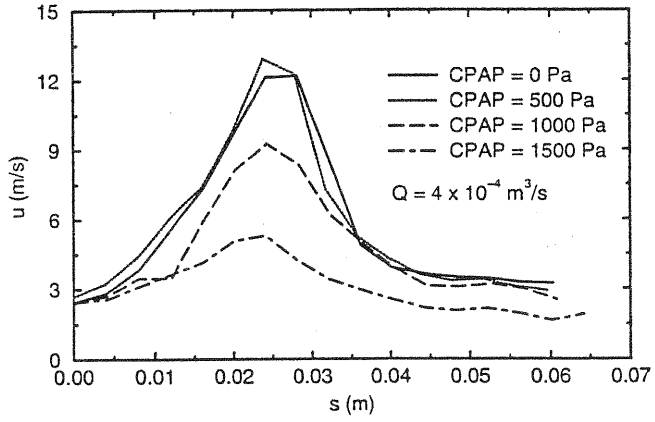

Fig. 8(*b*) Effect of CPAP on the average velocities in pharynx

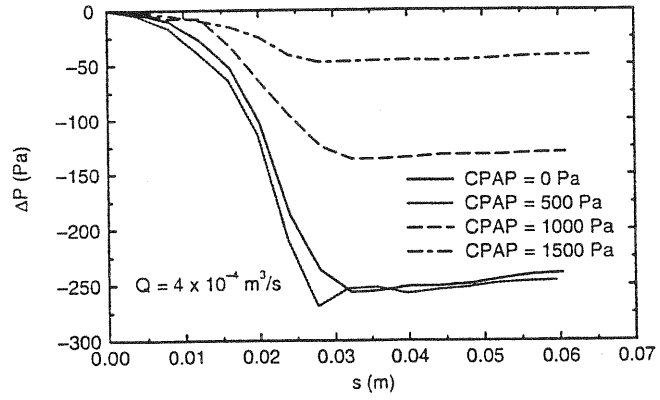

Fig. 8(*c*) Effect of CPAP on the pressure drop in pharynx

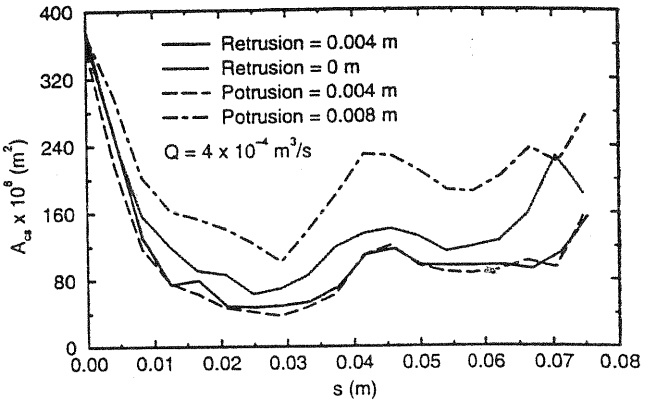

Fig. 9(*a*) Effect of dental repositioning devices on the cross-sectional area of pharynx

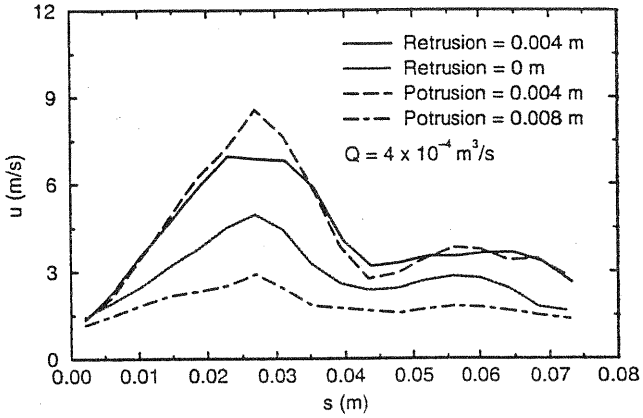

Fig. 9(*b*) Effect of dental repositioning devices on the average velocities in pharynx

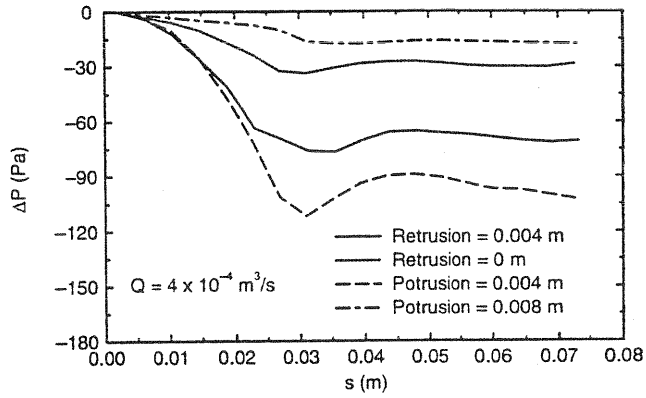

Fig. 9(*c*) Effect of dental repositioning devices on the pressure drop in pharynx

figures show that for CPAP ≤ 1000 Pa, the effect of the CPAP on the change in the cross-sectional areas is subtle. As seen in Fig. 8(*b*), the average velocity profile shows a sharp flow acceleration in the anterior portion of the pharynx with the peak air velocity reaching values as high as 14 m/s. This strong acceleration is caused by the large reduction in the pharynx lumen size and leads to significant pressure drop. A deceleration effect is also seen in Fig. 8(*b*) as the air velocity decreases in the posterior portion of the pharynx due to enlargement of the lumen. Figure 8(*c*) shows that even though the change in cross-sectional area is small, the corresponding change in the pressure drop is large. Since the cross-sectional area increases with CPAP (for CPAP ≥ 500 Pa), the pressure drop will decrease with increasing values of CPAP. The location of minimum intra-

/ 9711$$ju14 04-13-98 22:42:43 asmel ASME: J Bio Eng

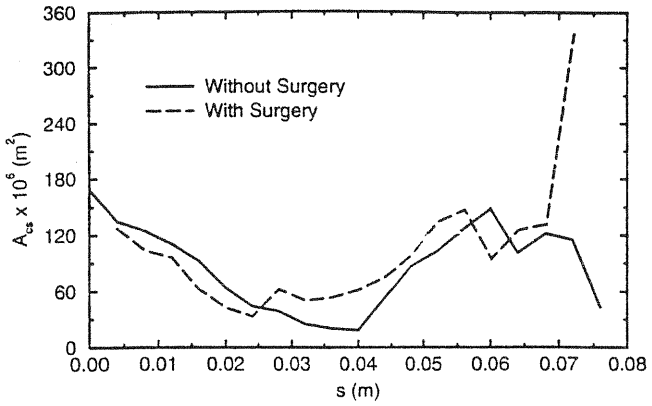

Fig. 10(*a*) Effect of surgery on the cross-sectional area of pharynx

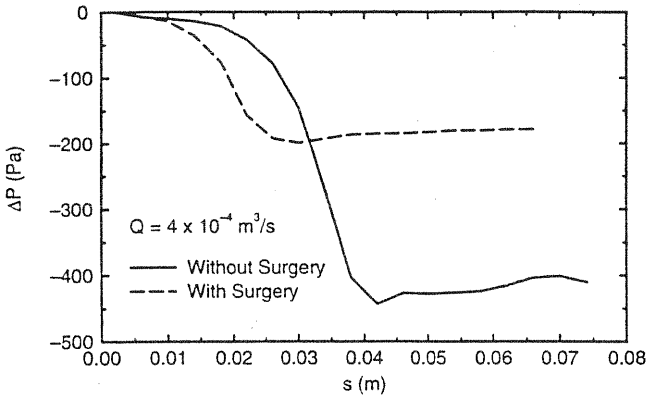

Fig. 10(*b*) Effect of surgery on the pressure drop in pharynx

luminal pressure lies at the point of minimum cross-sectional area. This is because the pressure drop due to fluid acceleration is largest at the smallest cross section. The results also show a small pressure drop recovery in the later portion of the airway caused by the flow deceleration; however, the magnitude of this recovery is small compared to the amount of pressure drop due to turbulence, flow acceleration, and frictional losses combined.

The effect of mandibular repositioning devices on the lumen cross-sectional area, average velocities, and the pressure drop for a single patient is shown in Figs. 9(*a*), 9(*b*), and 9(*c*), respectively. These figures again demonstrate that even though the change in cross-sectional area is marginal, there is a significant effect on the pressure drop. For instance, the change in the area between the cases where the jaw is retruded by 4×10^{-3} m and the case where it is potruded by 4×10^{-3} m is marginal, whereas a significant change in the pressure drops is observed for these two cases. For the case with 8×10^{-3} m jaw potrusions, the lumen cross-sectional area is considerably enlarged leading to a sharp decrease in the pressure drop.

The effect of surgery on the cross-sectional areas and the pressure drop is shown in Figs. 10(*a*) and 10(*b*). These figures clearly highlight reduction in the pressure drop caused by the surgical enlargement of the pharynx lumen. Even though recirculation regions exist for the surgically altered pharynx case (as seen in Fig. 7), their effect on the pressure drop is small since the strength of the recirculation is weak for this particular case. However, in general, the occurrence of such recirculation zones could trigger transition to turbulence and further increase the pressure drop.

Conclusions

A three-dimensional numerical simulation of airflow in an anatomically accurate human pharynx was conducted to calculate airflow characteristics. The $k-\epsilon$ turbulence model was found to be the most appropriate for simulating the transitional flow, encountered in the pharynx. The results showed that the pressure drop in the pharynx lies in the range 200–500 Pa. The minimum intraluminal pressure occurred in the smallest cross section where the airway is likely to collapse, leading to OSA. The onset of turbulence had a large effect on the pressure drop and it accounted for as much as 40 percent of it. In addition, the pressure drop varied approximately as the square of the inspiratory flow rate. The effect of three treatment therapies (CPAP, mandibular repositioning devices, and surgery) on the airway morphology and the resulting airflow characteristics were investigated and compared. The results showed that a subtle change in the morphology caused by these therapies can have a large effect on the pressure drop, since the flow is in the transitional regime. Weak flow recirculation zones caused by abrupt changes in the morphology due to surgery were also detected. Finally, the results presented here can serve as a basis for comparison with the more realistic study of dynamically coupled, soft-tissue airflow interactions.

Acknowledgments

This study was funded by the National Institute of Health under SBIR/STTR grant number 1-R41-NS34585-01. This support is gratefully acknowledged.

References

Carew, E. O., and Pedley, T. J., 1997, "An Active Membrane Model for Peristaltic Pumping: I—Periodic Activation Waves in an Infinite Tube," ASME JOURNAL OF BIOMECHANICAL ENGINEERING, Vol. 119, pp. 66–76.

Elad, K., Roger, D. K., and Shapiro, A. H., 1987, "Choking Phenomena in Lung-like Model," ASME JOURNAL OF BIOMECHANICAL ENGINEERING, Vol. 109, pp. 1–9.

Elad, D., Liebenthal, R., and Einav, S., 1991, "Simulation of Air Flow in the Human Nasal Cavity," *Proc. 4th FIDAP Users' Conference*, Evanston, IL.

FIDAP, 1993, Users' and Theory Manuals, Version 7.0, Fluid Dynamics International, Evanston, IL.

Hahn, I., 1992, "Modeling Nasal Airflow and Olfactory Mass Transport," Ph.D. Thesis, University of Pennsylvania, Philadelphia, PA.

Hanjalic, K., 1994, "Advanced Turbulence Closure Models: A View of Current Status and Future Prospects," *International Journal of Heat and Fluid Flow*, Vol. 15, No. 3, pp. 178–203.

Isono, S., and Remmers, J. E., 1993, "Anatomy and Physiology of Upper Airway Obstructions," *Principles and Practice of Sleep Medicine*, Kryger, M. H., Roth, T., and Dement, W. C., eds., W. B. Saunders Company, Philadelphia, PA, pp. 642–655.

Kamm, R. D., and Pedley, T. J., 1989, "Flow in Collapsible Tubes: A Brief Review," ASME JOURNAL OF BIOMECHANICAL ENGINEERING, Vol. 111, pp. 177–179.

Keyhani, K., Scherer, P. W., Hahn, I., and Mozell, M. M., 1993, "Modeling of Airflow in the Human Nasal Cavity," *Advances in Bioengineering*, ASME BED-Vol. 26, pp. 299–302.

Launder, B. E., and Spalding, D. B., 1974, "The Numerical Computation of Turbulent Flow," *Computer Methods in Applied Mechanics and Engineering*, Vol. 3, pp. 269–289.

Leger, D., 1994, "The Cost of Sleep-Related Accidents: A Report for the National Commission on Sleep Disorders," *Sleep*, Vol. 17, No. 1, pp. 84–93.

Luo, X. Y., and Pedley, T. J., 1996, "A Numerical-simulation of Unsteady-Flow in a 2-dimensional Collapsible Channel," *J. Fluid Mech.*, Vol. 314, pp. 191–225.

Lynch, D. G., Waters, S. L., and Pedley, T. J., 1996, "Flow in a Tube With Nonuniform, Time-Dependent Curvature—Governing Equations and Simple Examples," *J. Fluid Mech.*, Vol. 323, pp. 237–265.

National Commission on Sleep Disorders Research, 1993, "Wake-up America: A National Sleep Alert," Vol. 1, National Institute of Health, Bethesda, MD.

Pack, A. I., 1993, "Identifying Patients With Sleep Apnea Syndrome," *Sleep Medicine Review*, Vol. 1, No. 4.

Rodi, W., 1980, "Turbulence Models and Their Application in Hydraulics," International Association for Hydraulic Research, Netherlands.

Schmidt, R. C., and Patankar, S. V., 1987, "Prediction of Transition on a Flat Plate Under the Influence of Free-Stream Turbulence Using Low-Reynolds-Number Two-Equation Turbulence Model," ASME Paper No. 87-HT-32.

Tutty, O. R., and Pedley, T. J., 1994, "Unsteady-Flow in a Nonuniform Channel—A Model for Wave Generation," *Phys. Fluids*, Vol. 6, pp. 199–208.

White, F. M., 1986, *Fluid Mechanics*, McGraw-Hill, New York, pp. 305–310.

Wilcox, D. C., 1994, "Simulation of Transition With a Two-Equation Turbulence Model," *AIAA Journal*, Vol. 32, No. 2, pp. 247–255.